ACCEPTED AUTHOR MANUSCRIPT of
I.V. Alenkina, M.I. Oshtrakh, Z. Klencsár, E. Kuzmann, A.V. Chukine, V.A. Semionkin:
^{57}Fe Mössbauer Spectroscopy and Electron Paramagnetic Resonance Studies of Human Liver Ferritin, Ferrum Lek and Maltofer®, *Spectrochimica Acta Part A: Molecular and Biomolecular Spectroscopy* 130 (2014) 24-36. (http://dx.doi.org/10.1016/j.saa.2014.03.049)
NOTICE: this is the author's version of a work that was accepted for publication in Spectrochimica Acta Part A: Molecular and Biomolecular Spectroscopy. Changes resulting from the publishing process, such as peer review, editing, corrections, structural formatting, and other quality control mechanisms may not be reflected in this document. Changes may have been made to this work since it was submitted for publication. A definitive version was subsequently published as *Spectrochimica Acta Part A: Molecular and Biomolecular Spectroscopy* **130** (2014) 24-36.

^{57}Fe MÖSSBAUER SPECTROSCOPY AND ELECTRON PARAMAGNETIC RESONANCE STUDIES OF HUMAN LIVER FERRITIN, FERRUM LEK AND MALTOFER®

I.V. Alenkina[a,b], M.I. Oshtrakh[a,b,✉], Z. Klencsár[c], E. Kuzmann[d], A.V. Chukin[e], V.A. Semionkin[a,b]

[a]Department of Physical Techniques and Devices for Quality Control and [b]Department of Experimental Physics, Institute of Physics and Technology, Ural Federal University, Ekaterinburg, 620002, Russian Federation;
[c]Institute of Molecular Pharmacology, Research Centre for Natural Sciences, Hungarian Academy of Sciences, Pusztaszeri út 59-67, Budapest, 1025, Hungary;
[d]Institute of Chemistry, Eötvös Loránd University, Budapest, Hungary;
[e]Department of Theoretical Physics and Applied Mathematics, Institute of Physics and Technology, Ural Federal University, Ekaterinburg, 620002, Russian Federation

[✉]Corresponding author, E-Mail: oshtrakh@gmail.com (Department of Physical Techniques and Devices for Quality Control, Institute of Physics and Technology, Ural Federal University, Ekaterinburg, 620002, Russian Federation)

Abstract

A human liver ferritin, commercial Ferrum Lek and Maltofer® samples were studied using Mössbauer spectroscopy and electron paramagnetic resonance. Two Mössbauer spectrometers have been used: (i) a high velocity resolution (4096 channels) at 90 and 295 K, (ii) and a low velocity resolution (250 channels) at 20 and 40 K. It is shown that the three studied materials have different superparamagnetic features at various temperatures. This may be caused by different magnetic

anisotropy energy barriers, sizes (volume), structures and compositions of the iron cores. The electron paramagnetic resonance spectra of the ferritin, Ferrum Lek and Maltofer® were decomposed into multiple spectral components demonstrating the presence of minor ferro- or ferrimagnetic phases along with revealing marked differences among the studied substances. Mössbauer spectroscopy provides evidences on several components in the measured spectra which could be related to different regions, layers, nanocrystallites, etc. in the iron cores that coincides with heterogeneous and multiphase models for the ferritin iron cores.

Keywords: *Mössbauer spectroscopy; Electron paramagnetic resonance; Ferritin, Maltofer®, Ferrum Lek*

1. INTRODUCTION

Iron metabolism is essential for a large number of biological processes and its disturbance may result in the iron deficiency anemia [1]. Maltofer® and Ferrum Lek are two commercial pharmaceuticals used for anemia treatment. They consist of polynuclear nanosized ferric cores surrounded by noncovalent bonded polymaltose molecules. They represent a large stable complex (molecular weight of about 5000 Da) which do not release free iron radicals. Ferritin, the main iron storage protein in the body, consists of 24 protein subunits shell surrounding a cavity of 8 nm diameter in which the ferrihydrite-like iron core is located [2–4], whereas, the iron cores in Maltofer® and Ferrum Lek are ferric hydrous oxides in the form of β–FeOOH (akaganéite) with a similar or slightly larger size. Thus, Ferrum Lek and Maltofer® can be considered as ferritin analogues.

The iron core structures in iron storage proteins from different living systems or even different organs and tissues within one body vary as the iron core formation depends on different conditions (see, for instance, [2–5]). There were various studies of ferritin mineral cores suggested different models for the iron core structure, for instance, from one crystallite to several crystallites (see for review [6]). Some structural studies using electron nanodiffraction and high resolution electron microscopy indicated that the iron cores in ferritin molecules consist of single crystals of ferrihydrite or hematite and magnetite [7–9]. The heterogeneous iron core structure was suggested in [10] on the basis of X-ray absorption spectroscopy. Recently the polyphasic iron core composition consisted of ferrihydrite, magnetite and hematite was suggested in [11] on the basis of transmission electron microscopy, X-ray absorption near edge spectroscopy and other methods. In this work a ferrihydrite-magnetite core-shell structure was suppose. However, the thermal effect of 100–200 keV electron beam irradiation of ferritin with thermal decomposition of ferrihydrite was not taken into account in these studies as it was demonstrated in [12, 13] (earlier studies of thermal ferrihydrite decomposition using X-ray diffraction and infrared spectroscopy [14] and Mössbauer spectroscopy [15] demonstrated hematite formation). Further study of ferritin iron core using scanning transmission electron microscopy under controlled electron fluence permitted the authors of [16] to suggest a cubic-like core structure with eight subunits forming by closely packed crystalline structures of ferrihydrite surrounding with the loosely packed Fe^{3+}. The surface of each core subunit in this model is disordered facilitating dynamic iron load and release activities. In contrast, in the study of ferritin using scanning transmission electron microscopy with modeling the authors suggested that the ferritin mineral core is a hollow particle [17]. Magnetic study of ferritin demonstrated features which permitted the authors to suggest so-called core-shell model [18]. In this study an unusual dependence of magnetization versus field was observed. This dependence contained two components which were related to paramagnetic and antiferromagnetic parts of the core. This model of ferritin iron core proposes an interior antiferromagnetic iron core structure with Néel temperature (T_N) > 310 K surrounded by an amorphous surface layer with a lower T_N value, where the exchange forces are not strong enough to maintain the antiferromagnetic order. Similar behavior of isothermal magnetization curves were obtained for ferritin and its analogue iron dextran [19–24]. Recently a three-phase iron core structure for ferritin was suggested in [25] on the basis of new fitting model for the horse spleen ferritin magnetization curves and above mentioned electron nanodiffraction ferritin studies [7, 11]. These phases were: 60–80 % of ferrihydrite, 15–25 % of maghemite/magnetite, and 1–10 % of hematite.

Mössbauer spectroscopy is used for the study of ferritins and its pharmaceutical analogues for a long time (see for review [24, 26]). Ferritin taken from different organs, tissues, bodies as well as from the same source may differ in the number of Fe atoms and iron–inorganic phosphate ratio, the iron core structure and/or size, resulting in different superparamagnetic behavior and variations in Mössbauer parameters. In the study of ferritin with a lower iron loading (smaller core sizes), where the surface to volume ratio is higher, the authors [27, 28] applied the core-shell model to fit the Mössbauer spectra of the ferritin, assuming two paramagnetic components at high temperatures and two magnetic ones at low temperatures related to the surface and interior core. However, application of two magnetic and/or two paramagnetic components only, is insufficient in general to fit adequately the Mössbauer spectra of ferritin and related pharmaceutical compounds (see [29–32]).

Electron paramagnetic resonance (EPR) spectroscopy is also a well suited method to study ferritin and its pharmaceutical analogues. By means of EPR one can distinguish between two kinds of ferric ions: (i) solitary ions which lead to a peak with an effective *g*-factor of $g_{\mathrm{eff}} \approx 4.3$ and are bound to the ferritin protein shell and (ii) those which contribute to a broad spectral component at $g_{\mathrm{eff}} \approx 2$ and are accumulated within the protein. The latter ones contribute to the nanosized superparamagnetic ferric core [33–36]. EPR spectra demonstrate that smaller and larger ferritin core particles can also be differentiated on the basis of their apparent magnetic anisotropy field that is observable in their EPR spectra [35].

Recently, we have demonstrated that an increase in the velocity resolution of a Mössbauer spectrometer improve significantly the analysis of measuring spectra of ferritin and Imferon, an iron dextran analogue of ferritin [37]. Mössbauer spectrometer with a saw-tooth shape velocity reference signal formed using quantification with 4096 steps enables to deduce hyperfine parameters with significantly smaller instrumental (systematic) errors and to fit the complex spectra with more reliable results. That is in contrast to conventional spectrometers operate with triangular or sinusoidal velocity reference signals which formed using quantification up to 1024 steps (for similar signal-to-noise ratio in the spectra). Biomedical applications of the Mössbauer spectroscopy with a high velocity resolution clearly demonstrated these advantages [38–43]. In order to get further information about the iron core structure by comparison of human liver ferritin, Ferrum Lek and Maltofer®, we report here the ^{57}Fe Mössbauer spectra preformed at 4 different temperatures. The high temperature spectra (at 90 and 295 K) were measured by the high velocity resolution Mössbauer spectrometer, whereas the low temperature spectra (at 20 and 40 K) were measured by the low velocity resolution spectrometer. We also report EPR studies performed at various temperatures.

2. MATERIALS AND EXPERIMENTAL METHODS

The lyophilized human liver ferritin was obtained from the Russian State Medical University, Moscow, Russian Federation. Its preparation process is described in Ref [44]. For the present studies 100 mg powder sample was used. Commercial samples of Maltofer® (Vifor Inc., Switzerland) and Ferrum Lek (Lek, Slovenia) tablets were used as ferritin analogues. Each tablet contained 100 mg of Fe and 1/3 of a tablet was powdered for sample preparation. The absorbers of 10 mg Fe/cm^2 were prepared for Mössbauer studies. Powder X-ray diffraction (XRD) patterns for all samples were carried out by using PANalytical X'pert PRO diffractometer with CuK_α radiation at the Ural Federal University, Ekaterinburg. These samples were studied by Quanta 200 scanning electron microscopy (SEM) with energy dispersion spectroscopy (EDS) for chemical analysis and by magnetic measurements using commercial SQUID magnetometer MPMS-5S (Quantum Design) at the Hebrew University, Jerusalem. Thermogravimetry (TG) studies were carried out using SETSYS Evolution (Setaram) at the Institute of Solid State Chemistry, Ural Branch of the RAS, Ekaterinburg. The ferritin powder was analyzed by MORGAGNI 268D transmission electron microscopy (TEM) at the Research Center for Natural Sciences, HAS, Budapest.

Mössbauer spectra with a high velocity resolution were measured at the Ural Federal University (Ekaterinburg) using an automated precision Mössbauer spectrometric system built on the base of the SM-2201 spectrometer with a saw-tooth shape velocity reference signal formed by the digital-analog convertor using quantification with 4096 steps. Details and characteristics of this spectrometer and the system are given elsewhere [45–47]. The ^{57}Co in rhodium matrix source of about 1.0×10^9 Bq (Ritverc GmbH, Saint-Petersburg) was used at room temperature. Spectra at 295 and 90 K were measured in transmission geometry with moving absorber in the liquid nitrogen cryostat and registered in 4096 channels. Statistical counts were in the range of 4.1×10^5 – 2.7×10^6 counts per channel and the signal-to-noise ratios were in the range from 96 to 134. The spectra were fitted using the UNIVEM-MS program with a least squares procedure and the Lorentzian line shape. Parameters determined for the measured spectra were: isomer shift, δ, quadrupole splitting, ΔE_Q, line width, Γ, relative subspectrum area, S, and normalized statistical criteria of fitting quality χ^2. As criteria for choosing the best fits, a differential spectrum, χ^2 and a physical meaning of the spectral parameters were considered. The instrumental (systematic) error for each spectrum point and for the hyperfine parameters were ±0.5 and ±1 channel, respectively [47]. The velocity resolution in the spectra was ~0.001 mm/s per channel. The error of S did not exceed 10 %. If an error calculated with the fitting procedure (fitting error) for these parameters exceeded the instrumental (systematic) error we used the larger error instead. Values of the isomer shifts are given relative to that of α–Fe at 295 K.

Additionally, the Mössbauer spectra of the studied samples were measured with the low velocity resolution at 40 and 20 K using a conventional (KFKI type) spectrometer with the triangular velocity reference signal formed using quantification with 1024 steps, and an APD closed cycle refrigerator at the Eötvös Loránd University, Budapest. Each spectrum recorded on the direct and the reverse motion was registered in 500 channels using twofold increase of the multichannel analyzer time window in comparison with the time of one velocity step. To exclude an effect of a residual parabolic distortions and a folding procedure – which may distort the spectra (see [47]) –

the analysis of these spectra was carried out only on the data recorded during the direct motion measurement in 250 channels. The ~1.8×10^9 Bq ^{57}Co in rhodium matrix source (Ritverc GmbH, Saint-Petersburg) was used at room temperature. The statistical counts for the spectra of the human liver ferritin and its pharmaceutical models measured at 40 and 20 K were in the range of 1.6×10^5 – 1.6×10^6 counts per channel, and the signal-to-noise ratio was in the range between 31 and 55. The spectra were also computer fitted using the UNIVEM-MS program in the same manner as mentioned above with additional determination of magnetic hyperfine field, H_{eff} and accounting the parabolic distortion of the spectra. The instrumental (systematic) error for each spectrum point and for the hyperfine parameters were ±0.5 and ±1 channel, respectively, while that of the line width was ±2 channels (see [47]). The velocity resolution in the spectra without the folding was ~0.11 mm/s per channel. It should be noted that in spite of the low velocity resolution of the KFKI spectrometer it was of great help for Mössbauer spectra measurement at 40 and 20 K which are not available using SM-2201 spectrometer.

EPR spectra on powder ferritin, Maltofer® and Ferrum Lek were recorded at room temperature using a Bruker ElexSys E500 X-band EPR spectrometer at the Research Centre for Natural Sciences, HAS, Budapest. A modulation frequency of 100 kHz was used. The applied modulation amplitude and the microwave power for ferritin were 10 G and ~20 mW, respectively, whereas they were 5 G and ~10 mW for Ferrum Lek and Maltofer®. Separate measurements were performed under identical conditions in an empty sample holder (quartz tube) in order to determine the background level of intensities as a function of the measuring DC magnetic field, *B*. The background was subtracted from the spectra measured on the samples prior to their analysis. In order to detect the signal of non-aggregated paramagnetic iron ions in ferritin, low-temperature measurements were carried out on the ferritin sample in the range of 150–290 K with modulation amplitude and microwave power of 10 G and ~10 mW, respectively.

3. RESULTS AND DISCUSSION

3.1. Characterization of the samples using XRD, SEM, TEM, thermogravimetry and magnetization measurements

SEM image of a Maltofer® sample is shown in Fig. 1a. This image demonstrates agglomerates of Maltofer® macromolecules in a powder at magnification of ×600. However, the size of the polymaltose shell excludes interparticle interaction for different iron cores in the sample. Elemental composition in Ferrum Lek and Maltofer® samples obtained using SEM with EDS is given in Table 1. The chemical composition for the main elements was slightly different in both pharmaceutical samples. XRD patterns for human liver ferritin, Ferrum Lek and Maltofer® are shown in Fig. 1b–d. These patterns reflect complex phase composition of studied samples due to the presence of large amounts of crystallized salts in the lyophilized ferritin sample and due to different ingredients in Ferrum Lek and Maltofer® tablets. Nevertheless, it is possible to distinguish low intensity peaks corresponding to ferrihydrite in human liver ferritin and to akaganéite in Ferrum Lek and Maltofer®. TEM analysis of the studied human liver ferritin sample demonstrated that the iron cores can be considered as spherically-shaped uniform nanoparticles with a narrow size distribution between 4 and 6 nm (Fig. 2a,b). In contrast, iron cores in Ferrum Lek and Maltofer® were not well identified probably due to additional components in tablets (Fig. 2c,d). However, recently the study of Ferrum Lek in aqueous suspension using TEM carried out in [48] demonstrated ellipsoid-shaped iron cores with average diameter of ~6 nm. If Maltofer® image in Fig. 2d is related to the iron cores, the morphology of two ferritin analogues is different.

The results of thermogravimetry of human liver ferritin, Ferrum Lek and Maltofer® samples are shown in Fig. 3. The heat flow and mass lost curves look similar to each other, however, the remanent mass for Ferrum Lek and Maltofer® (~25 % and ~23 %, respectively) was smaller than that for human liver ferritin (~35 %). These data were used for magnetization measurements. Zero field cooled and field cooled (ZFC and FC) magnetization curves for human liver ferritin, Ferrum Lek and Maltofer® samples are shown in Fig. 4a–c. These data were in agreement with previous studies of other ferritins and its pharmaceutical analogue iron dextran complex (see, for instance, [20, 24]). The isothermal magnetization curves of Ferrum Lek and Maltofer® are shown in Fig. 4d,e. The obtained curves for both iron-polymaltose complexes are very similar. The coercive fields at 5 K are –400 Oe for Ferrum Lek and –440 Oe for Maltofer®. Isothermal magnetization curves were also similar to the published results (see, for instance, [18, 24]) on the other ferritins and demonstrated a slope as a result of saturation magnetization curve and additional linear component (Fig. 4f). Previously this fact was interpreted as two phase composition of the ferritin iron core (see, for instance, [18–24]). Our results for Ferrum Lek and Maltofer® demonstrated similar magnetic behavior as for human liver ferritin, i.e. both isothermal magnetization curves contain saturation magnetization part (superparamagnetic) and linear part (paramagnetic or superantiferromagnetic). On the basis of the similar magnetic feature a core-shell model of the ferritin iron core was developed [18] and applied for the evaluation of the ferritin Mössbauer spectra [24, 27, 28].

3.2. Mössbauer spectroscopy

3.2.1. Mössbauer spectroscopy with the high velocity resolution at 295 and 90 K

The Mössbauer spectra of the human liver ferritin, Maltofer® and Ferrum Lek measured with the high velocity resolution at 295 K show similar patterns, as shown in Fig. 5a,c,e. In the present study we applied a heterogeneous iron core model for the fit of Mössbauer spectra – introduced elsewhere [37, 49, 50] – i.e. the spectra were analyzed using several quadrupole doublets. The best fits of these spectra were obtained with 4 quadrupole doublets for the ferritin and 5 quadrupole doublets for both iron-polymaltose complexes Maltofer® and Ferrum Lek. It should be noted that the best fit was determined on the basis of linear shape (within the statistical error) of differential spectrum and minimal χ^2 value. For instance, in the case of the 295 K human liver ferritin spectrum (Fig. 5a), inserted images of differential spectra obtained from this spectrum fits using one, two and three quadrupole doublets clearly show deviations from the linear shape of differential spectra beyond the statistical errors. Moreover, the values of χ^2 were 5.713, 1.621, 1.154 and 1.067 for the one, two, three and four quadrupole doublets fits, respectively (standard deviation for χ^2 is: σ=0.022). The Mössbauer spectra of the ferritin, Maltofer® and Ferrum Lek measured at 90 K are presented in Fig. 5b,d,f. The same number of the quadrupole doublets as in the case of spectra recorded at 295 K was necessary to obtain the best fits that can be regarded in favor of the chosen model. In the previous study we fitted the previously measured 295 and 90 K spectra of the same samples independently and observed unexpected differences in the corresponding Mössbauer parameters [49]. That is why we applied consistent fit for the spectra of the same samples measured at two temperatures in the present study. The spectra of each sample measured at 295 and 90 K were fitted using corresponding consistent model (maintaining similar constrains for the corresponding Mössbauer parameters at both temperatures). The best fit Mössbauer parameters obtained in that way are given in Table 2. We have surprisingly found an increase in the line widths of the spectral components at 90 K. Some small line broadening related to the cryostat vibrations at this temperature was shown in [46]. However, in the present case the line broadening cannot be related to the cryostat vibrations only and requires a separate study that will be published elsewhere to elucidate whether or not this result is related to a relaxation process.

It is well-known that quadrupole splitting and electric field gradient are very sensitive to the local microenvironment of the ^{57}Fe nucleus. Therefore, the observed differences beyond the errors in ΔE_Q values for some corresponding quadrupole doublets obtained for the Mössbauer spectra of human liver ferritin, Maltofer® and Ferrum Lek given in Table 2 may indicate that Fe^{3+} ions in the iron cores of human liver ferritin and its analogues had some small stereochemical variations related, for instance, to differences in oxygen and iron atoms packing in the core.

Though the Mössbauer spectra of both iron-polymaltose complexes Maltofer® and Ferrum Lek measured at 295 and 90 K were fitted with the same number of the quadrupole doublets, the values of the hyperfine parameters turned out to be different for the spectral components with similar relative areas. The relative areas of the components 1–5 obtained at 295 and 90 K (see Table 2 and Fig. 6) turned out to be different beyond the error limit for both Maltofer® and Ferrum Lek while the relative areas of corresponding components were the same within the error at 295 and 90 K for each sample. Consequently, one can conclude that the regions/layers of the iron cores related to these components may differ as far as their size, the ^{57}Fe content, degree of crystallinity, density of atoms package, etc. is concerned. This finding indicated the existence of the iron core differences in the two iron-polymaltose complexes that possibly may be related to different manufacturing processes involved in their production.

According to the previous finding of Funk et. al. [29], the Mössbauer spectrum of the iron-polymaltose complexes measured with the low velocity resolution demonstrated magnetic components in addition to paramagnetic one at the temperature of liquid nitrogen. Therefore, we additionally performed Mössbauer spectra measurements of Maltofer® and Ferrum Lek with the high velocity resolution at 90 K in a large velocity range and compared our results with those presented in [29] (see Fig. 7). However, we did not observe magnetic splitting in our spectra. To account for the previous finding we can exclude aging effects that might cause an aggregation and/or a crystallization of the iron cores, resulting in an increased blocking temperature. The iron cores in the presently studied iron-polymaltose complexes are apparently characterized by a smaller magnetic anisotropy energy barrier than that in the iron cores of the complexes studied in [29]. The difference is presumably due to a smaller core-size in our case.

3.2.2. Mössbauer spectroscopy with the low velocity resolution at 40 and 20 K

The Mössbauer spectra of the human liver ferritin, Maltofer® and Ferrum Lek measured with the low velocity resolution spectrometer at 20 K are shown in Fig. 8a-c. A comparison of these spectra gives evidence that magnetically split components prevail in the spectra of the pharmaceutical models while the spectrum of the ferritin consists of a major paramagnetic component and a small magnetic one. It should be noted that a parabolic distortion in the 20 K ferritin spectrum may mask a small magnetic component; the value of χ^2=1.045 was obtained in the case of the fit without magnetic component while for the fit with a small magnetic component the value of χ^2 was equal to 1.028 (σ=0.066). Moreover, previous studies of other ferritin samples demonstrated the presence of the magnetic component at 20 K (see [51]). This finding indicated that the magnetic anisotropy energy barriers for the iron cores in the human liver ferritin and those in Maltofer® and Ferrum Lek were different. Furthermore, assuming the magnetic anisotropy constants were similar in the iron cores of the studied samples, one can conclude that the iron core size (volume) of the ferritin was somewhat smaller than that in Maltofer® and Ferrum Lek. A comparison of the Mössbauer spectra of Maltofer® and Ferrum Lek measured at 20 K (see Fig. 8b, c) showed, in fact, small differences. Therefore, these samples were additionally measured at 40 K and compared with the Maltofer® spectrum measured at 45 K as reported in [29] (Fig. 9). The 40 K Mössbauer spectra of Maltofer® and Ferrum Lek demonstrated also some differences. The results of the best fits of these spectra using individual magnetic and paramagnetic components are shown in Figs. 8 and 9 and the spectral parameters are given in Table 3. The 40 K spectra of Maltofer® and Ferrum Lek were fitted using 5 magnetic sextets and 2 quadrupole doublets while the 20 K spectra of Maltofer® and Ferrum Lek were fitted using 7 magnetic sextets and 1 quadrupole doublet. A further increase in the number of components during the fit led to the lack of physical meaning of the parameters or increase in χ^2-values. The 20 K Mössbauer spectrum of ferritin was fitted using 2 quadrupole doublets and 1 magnetic sextet. A comparison of the Mössbauer parameters obtained for Maltofer® and Ferrum Lek at 40 and 20 K showed evidence on some differences in the corresponding parameters. This finding may indicate the presence of the same number of corresponding regions/layers (grains, etc.) in the iron cores of Maltofer® and Ferrum Lek with different parameters, e. g. having a different size/volume (or number of Fe atoms) and the magnetic hyperfine field value. However, it is not possible to directly compare these results with those obtained for the 295 and 90 K spectra due to the different velocity resolution in the spectra.

Nevertheless, the results are compatible with the suggested heterogeneous iron core models which seem to be more adequate than the core-shell model [27, 28] for analysis of the Mössbauer spectra of the ferritin and its pharmaceutical analogues.

3.3. Mössbauer parameters and the iron core structure

The core-shell model proposed for the iron core of the ferritin [18] was used as a physical model when analyzing the ferritin Mössbauer spectra measured at various temperatures [27, 28]. However, heterogeneous and multiphase models were proposed for the ferritin iron cores [6–11, 16, 17, 25]. In the present work we continue the development of the heterogeneous iron core model on the basis of the Mössbauer spectra best fits [37, 49, 50]. Interactions between the iron cores should be neglected due to a protein shell shielding (see also [24, 52]). Therefore, the Mössbauer parameters can be analyzed in relation to the size and structure of the iron core. In this case we may assume that the doublets with the smallest quadrupole splitting obtained in the Mössbauer spectra measured at 295 and 90 K can be related to the internal region of the ferrihydrite type core with a higher degree of crystallinity and density of atoms packing. In contrast, the doublets with the largest quadrupole splitting can be related to the surface shell of the core with a less ordered structure. Therefore, if we consider the same recoilless fraction for various core regions/layers it is possible to estimate their contribution as follows: about 15–16 % of surface core shell, about 23–27 % of the next region/layer in the nanoparticle, about 31–35 % of a deeper internal regions/layer and about 26 % of an internal core area. The akaganéite type cores in Maltofer® and Ferrum Lek with a larger magnetic anisotropy energy than that in the human liver ferritin iron cores probably have a lager particle size (volume). Therefore, the Mössbauer spectra of Maltofer® and Ferrum Lek measured at 295 and 90 K could be fitted using 5 quadrupole doublets while those of the human liver ferritin were fitted using 4 quadrupole doublets only. Within the same assumption we can suggest five regions/layers of the iron core from the surface shell down to the internal core region/layer with relative contributions of about 5 %, 11%, 35–36 %, 35% and 15–16 %, respectively, for Maltofer®, and those of about 6–7 %, 9 %, 30 %, 33–34 % and 20–21 %, respectively, for Ferrum Lek. Unfortunately, it is not possibile to apply the model used for the analysis of 295 and 90 K spectra for a similar analysis of 40 and 20 K spectra due to different quality of the high and low velocity resolution spectra and their fits. Nevertheless, the fitting of the spectra of Maltofer and Ferrum Lek measured at 40 and 20 K also supports the heterogeneous iron core models by revealing multiple magnetic components (Fig. 9). We can assume that the smallest regions of the cores with a higher degree of crystallinity still remained paramagnetic at lower temperatures. The magnetic components (with decreasing magnetic field values) may be related to the regions/layers varied from a higher degree of crystallinity towards more amorphous surface layer. The possible effect of morphological differences for Maltofer® and Ferrum Lek iron cores should be studied additionally. Thus, the heterogeneous model with more than the core and shell only should be considered for further analysis of the Mössbauer spectra of the iron cores in ferritin and its analogues.

3.4. Electron paramagnetic resonance

Measured EPR spectra of human liver ferritin, Maltofer® and Ferrum Lek are shown in Fig. 10. The EPR spectrum of human liver ferritin displays a broad absorption signal centered near $g \approx 2$, which agrees with corresponding results found previously for horse spleen ferritin [33] and human spleen ferritin [34]. The width of the signal is presumably contributed to by inhomogeneous broadening caused by the disordered nature of the anisotropy axes of weakly ferrimagnetic substances such as the ferrihydrite core of ferritin [53], as well as by a distribution in the size of the ferrimagnetic core particles. Namely, as superparamagnetic relaxation of magnetic nanoparticles results in an apparent reduction of the effective anisotropy field depending on the particle size, anisotropy energy density and temperature [54], at the same temperature particles being of the same kind but having different volumes will sense a different fraction of their magnetic anisotropy field, and will, therefore, result in an EPR signal centered at a different apparent g factor and characterized by a different magnitude of anisotropy broadening. As shown in [35] larger ferrimagnetic particles of ferritin may produce a broad signal at lower resonance fields.

Fitting the EPR spectrum of human liver ferritin to a single Lorentzian derivative (not shown) results in an effective spectroscopic splitting factor of $g_{eff} \approx 2.04$ and an apparent FWHM line width of ~2.3 kG, but with a residual that suggests the presence of more than one subcomponent. An acceptable fit of the main spectrum feature can be achieved by applying at least three subcomponents as shown in Fig. 10. The component with the largest (~76.5 %) relative area fraction (F_a) displaying a large apparent peak-to-peak width of Γ_{pp} (F_a)≈2.61 kG represents the theoretical model of a random powder of particles with uniaxial magnetic anisotropy subject to an effective magnetic anisotropy field of ~1 kG and an intrinsic Lorentzian FWHM line width of ~3.9 kG along with an intrinsic g factor of $g_{eff}(F_a)$=2.093(5). Due to the large intrinsic width and the relatively low anisotropy field, the value of $g_{eff}(F_a)$ is close to the apparent $g_0(F_a)$≈2.1 spectroscopic splitting factor that corresponds to the maximum of absorption (i.e. zero crossing of the derivative of absorption considering also the baseline) represented by the F_a component (via the relationship $g_0 = hf / B_0\mu_B$ where f is the measuring frequency, μ_B is the Bohr magneton, h is the Planck constant and B_0 is the resonance magnetic field that results in the maximum of absorption). On the basis of its g factor and its rather large line width, component F_a bears close similarity with the EPR spectrum reported for natural inorganic goethite [55] displaying g_0≈2.09 and Γ_{pp} (F_a)≈2.79 kG, which suggests that the particles contributing to component F_a are, at least in part, composed of larger particles of ferric oxide-hydroxide. The F_a peak may, however, also be contributed to by ferrihydrite for which g_0=2.1 and Γ_{pp}≈850 G was recently reported [56]. The symmetric component F_b (accounting for ~23.3 % of the total spectral area) corresponds to a Lorentzian with $g_0(F_b)$=2.019(1) and $\Gamma_{pp}(F_b)$≈0.92 kG, which values are close to those (g_0≈2.02 and Γ_{pp}≈0.84 kG) observed for biogenic intracellular magnetite chains produced by the magnetotactic bacteria *Magnetospirillum magneticum* [55]. Again, one cannot exclude a contribution of ferrihydrite to component F_b, especially that the peak-to-peak width characteristic to ferrihydrite is close to that of F_b. The presence of magnetite along ferrihydrite, however, is a reasonable possibility considering the conception [51] that the biodegradation of ferrihydrite may lead to the biogenic magnetite crystals identified in human brain tissues. As shown in Fig. 11, in the EPR spectrum of human liver ferritin below room temperature a minor signal becomes discernible at $g \approx 4.2$, that can be attributed to non-aggregated, solitary high-spin Fe^{3+} ions bound on the ferritin protein shell to core-nucleation sites with rhombic symmetry [33, 35, 57].

To account for the main features of the EPR spectrum of the Maltofer® sample at least three Lorentzian subcomponents were needed. Component M_a, characterized by $g_0(M_a)\approx2.67$ and $\Gamma_{pp}(M_a)\approx2.89$ kG, gives ~94 % of the total absorption area. The splitting factor and the width of this component were in good agreement with corresponding values ($g_0\approx2.67$, $\Gamma_{pp}\approx2.74$ kG) reported for synthetic magnetite [55]. The remaining two components, M_b and M_c, represent respectively ~4 % and ~2 % of the total spectral area. They are characterized by $g_0(M_b)\approx2.32$, $\Gamma_{pp}(M_b)\approx0.52$ kG and $g_0(M_c)\approx2.90$, $\Gamma_{pp}(M_c)\approx0.41$ kG. It should be noted that EPR spectra recorded on different samples made of Maltofer® powder indicated that the samples may develop a texture that can also significantly affect the actual resonance field of the detected peaks and the associated spectral shape. However, mixing the measured sample with MgO powder in order to reduce texture preserved the essential features of the Maltofer® powder spectrum shown in Fig. 10.

The shape of the EPR spectrum of Ferrum Lek (Fig. 10) suggests that it can mainly be accounted for by magnetic anisotropy broadening. By assuming that the sample can be seen as a random powder of particles with similar size, we found that the assumption of cubic magnetic anisotropy provides a better fit of the spectrum than does the assumption of uniaxial anisotropy. The corresponding best fitting curve shown in Fig. 10 represents an intrinsic splitting factor of $g_{eff}\approx1.945$, a magnetic anisotropy field of $B_{a,eff}\approx-2.16$ kG and an intrinsic FWHM line width of ~2.45 kG. The spectrum is furthermore characterized by $\Gamma_{pp}\approx2.78$ kG and $g_0=2.145(6)$ demonstrating that when the anisotropy field is large, then the apparent g factor determined on the basis of the zero crossing of the derivative of absorption may be a poor approximation of the intrinsic g factor. On the basis of a comparison with the data in [55] by considering g_0 and Γ_{pp} alone natural inorganic goethite would be again the closest match to our data, but this assignment is unlikely as goethite is expected to display a positive uniaxial magnetocrystalline anisotropy [53]. At the same time, the ferrihydrite core of ferritin was found to exhibit negative uniaxial magnetic anisotropy [35] in agreement with its hexagonal crystal structure, though if this assignment was correct we would expect the model of uniaxial anisotropy to fit better the spectrum than that of cubic anisotropy. As it is known to exhibit negative first-order cubic magnetocrystalline anisotropy at room temperature, magnetite is also not excluded as the origin of the main feature in the EPR spectrum of Ferrum Lek.

4. CONCLUSIONS

Mössbauer spectroscopic study of the iron storage protein ferritin (from human liver) and its pharmaceutically important analogues Maltofer® and Ferrum Lek confirmed hypothesis on heterogeneous and probably multiphase iron core composition in the studied materials supposed on the basis of structural studies (for instance, [6, 10, 11, 16]). However, the present interpretation of our Mössbauer results could not support suggestions about a single crystalline iron core [7] or a hollow interior in the core [17]. Therefore, the heterogeneous model could be used for further development of the simple core-shell model in the fit of Mössbauer spectra of ferritin and its analogues by considering more than two regions/layers which can be derived from magnetization measurements. It was shown that the magnetic anisotropy energy barrier for the iron cores in the human liver ferritin and its pharmaceutical related compounds was different and, probably, the size (volume) of these nanosized iron cores was smaller in the ferritin than that in its analogues. Moreover, it was also observed that the iron cores in Maltofer® and Ferrum Lek could be considered as a complicated system with at least 5 regions or layers with differences in some of them that might have resulted from different manufacturing processes of Maltofer® and Ferrum Lek. In contrast, the studied human liver ferritin iron core may be considered as a system composed of at least 4 different regions and/or layers, etc.

According to the analysis of the EPR spectra one could clearly detect differences between the ferro- or ferrimagnetic phases of human liver ferritin and those of its actual pharmaceutical analogues Maltofer® and Ferrum Lek. Whereas the ferrimagnetic signal of ferritin seems to be realized by the residual ferrimagnetism of a ferric oxide-hydroxide phase, that of Ferrum Lek and especially of Maltofer® is likely to be mainly contributed to by an another type of magnetic compound. It is important to emphasize that as antiferromagnetic compounds are – apart from a possible residual ferrimagnetism – EPR silent, the actual overall composition of the studied samples may differ from that reflected by the EPR results that in the present study inform exclusively about the ferro-, ferri- and paramagnetic phases. For the same reason, the ^{57}Fe Mössbauer spectra of the samples (that also report about antiferromagnetic iron-containing phases) may well reflect a different composition while the phases contributing to the EPR spectra may actually have negligible contribution to the ^{57}Fe Mössbauer spectra, and vice versa. Nevertheless, the data obtained using EPR study of human liver ferritin, Maltofer® and Ferrum Lek demonstrated differences in the phase composition of the iron core related to the presence of minor ferro- or ferrimagnetic phases and contributed also to the heterogeneous and multiphase models of the iron core.

ACKNOWLEDGMENT

The authors wish to thank Prof. P.G. Prokopenko (Department of Biochemistry, Russian State Medical University, Moscow) for providing the human liver ferritin, Prof. S.M. Dubiel (Faculty of Physics & Applied Computer Science, AGH University of Science & Technology, Kraków) for providing the Ferrum Lek sample, Prof. I. Felner (Racah Institute of Physics, The Hebrew University, Jerusalem) for the scanning electron microscopy with energy dispersion spectroscopy and magnetization measurements and Dr. Péter Németh (Research Center for Natural Sciences, HAS, Budapest) for the transmission electron microscopy images. The authors are grateful to Prof. I. Felner for reading this manuscript and useful remarks. This work was supported by the basic financing from the Ministry of Science and Education of Russian Federation. I.V.A. is supported in part by the Ural Federal University development program for the young scientists' financial support. This work was carried out within the Agreement of Cooperation between the Ural Federal University (Ekaterinburg) and the Eötvös Loránd University (Budapest).

REFERENCES

[1] G.J. Handelman, N.W. Levin, Heart Fail Rev. 13 (2008) 393–404.

[2] E.C. Theil, Ann. Rev. Biochem. 56 (1987) 289–315.

[3] E.C. Theil, Cur. Opin. Chem. Biol. 15 (2011) 304–311.

[4] E.C. Theil, Inorg. Chem. 52 (2013) 12223−12233.

[5] E.R. Bauminger, P.M. Harrison, D. Hechel, I. Nowik, A. Treffry, Hyperfine Interact. 91 (1994) 835–839.

[6] W.H. Massover, Micron 24 (1993) 389–437.

[7] J.M. Cowley, D.E. Janney, R.C. Gerkin, P.R. Buseck, J. Struct. Biol. 131 (2000) 210–216.

[8] J.M. Cowley, Micron 35 (2004) 345–360.

[9] C. Quintana, J.M. Cowley, C. Marhic, J. Struct. Biol. 147 (2004) 166–178.

[10] M.-S. Joo, G. Tourillon, D.E. Sayers, E.C. Theil, Biol. Metals 3 (1990) 171–175.

[11] N. Galvez, B. Fernandez, P. Sanchez, R. Cuesta, M. Ceolin, M. Clemente-Leon, S. Trasobares, M. Lopez-Haro, J.J. Calvino, O. Stephan, J.M. Dominguez-Vera, J. Am. Chem. Soc. 130 (2008) 8062–8068.

[12] Y. Pan, A. Brown, R. Brydson, A. Warley, A. Li, J. Powell, Micron 37 (2006) 403–411.

[13] Y.-H. Pan, G. Vaughan, R. Brydson, A. Bleloch, M. Gass, K. Sader, A. Brown, Ultramicroscopy 110 (2010) 1020–1032.

[14] S.V.S. Prasad, V.S. Rao, J. Mater. Sci. 19 (1984) 3266–3270.

[15] I. Mitov, D. Paneva, B. Kunev, Thermochim. Acta 386 (2002) 179–188.

[16] Y.-H. Pan, K. Sader, J.J. Powell, A. Bleloch, M. Gass, J. Trinick, A. Warley, A. Li, R. Brydson, A. Brown, J. Struct. Biol. 166 (2009) 22–31.

[17] J.D. Lopez-Castro, J.J. Delgado, J.A. Perez-Omil, N. Galvez, R. Cuesta, R.K. Watt, J.M. Domınguez-Vera, Dalton Trans. 41 (2012) 1320–1324.

[18] R.A. Brooks, J. Vymazal, R.B. Goldfarb, J.W. Bulte, P. Aisen, Mag. Res. Med. 40 (1998) 227–235.

[19] S.H. Kilcoyne, R. Cywinski, J. Magn. Magn. Mater. 140–144 (1995) 1466–1467.

[20] S.H. Kilcoyne, A. Gorisek, J. Mag. Mag. Mater. 177–181 (1998) 1457–1458.

[21] P. Bonville, C. Gilles, Physica B, 304 (2001) 237–245.

[22] C. Gilles, P. Bonville, H. Rakoto, J.M. Broto, K.K.W. Wong, S. Mann, J. Mag. Mag. Mater. 241 (2002) 430–440.

[23] N.J.O. Silva, V.S. Amaral, L.D. Carlos, Phys. Rev. B 71 (2005) 184408.

[24] G.C. Papaefthymiou, Biochim. Biophys. Acta 1800 (2010) 886–897.

[25] J.H. Jung, T.W. Eom, Y.P. Lee, J.Y. Rhee, E.H. Choi, J. Mag. Mag. Mater. 323 (2011) 3077–3080.

[26] A.A. Kamnev, K. Kovács, I.V. Alenkina, M.I. Oshtrakh, In: V.K. Sharma, G. Klingelhofer, T. Nishida, (Eds.), Mössbauer Spectroscopy: Applications in Chemistry, Biology, Industry, and Nanotechnology. First Ed., John Wiley & Sons, Inc., 2013, pp. 272–291.

[27] F. Bou-Abdallah, E. Carney, N.D. Chasteen, P. Arosio, A.J. Viescas, G.C. Papaefthymiou, Biophys. Chem. 130 (2007) 114–121.

[28] G.C. Papaefthymiou, Nano Today 4 (2009) 438–447.

[29] F. Funk, G.J. Long, D. Hautot, R. Büchi, I. Christl, P.G. Weidler, Hyperfine Interact. 136 (2001) 73–95.

[30] M.I. Oshtrakh, O.B. Milder, V.A. Semionkin, L.I. Malakheeva, P.G. Prokopenko, J. Radioanal. Nucl. Chem. 269 (2006) 671–677.

[31] M.I. Oshtrakh, O.B. Milder, V.A. Semionkin, Hyperfine Interact. 181 (2008) 45–52.

[32] M. Miglierini, J. Dekan, M. Kopani, A. Lancok, J. Kohout, M. Cieslar, In: J. Tuček, L. Machala (Eds.), Proceedings of the International Conference “Mössbauer Spectroscopy in Materials Science 2012”, AIP Conference Proceedings, Melville, New York, 2012, 1489, pp. 107–114.

[33] E. Wajnberg, L.J. El-Jaick, M.P. Linhares, D.M.S. Esquivel, J. Mag. Res. 153 (2001) 69–74.

[34] N.D. Chasteen, B.C. Antanaitis, P. Aisen, J. Biol. Chem. 260 (1985) 2926–2929.

[35] M.P. Weir, T.J. Peters, J.F. Gibson, Biochim. Biophys. Acta 828 (1985) 298–305.

[36] P.M. Hanna, Y. Chen, N.D. Chasteen, J. Biol. Chem. 266 (1991) 886–893.

[37] M.I. Oshtrakh, O.B. Milder, V.A. Semionkin, Hyperfine Interact. 185 (2008) 39–46.

[38] M.I. Oshtrakh, V.A. Semionkin, O.B. Milder, E.G. Novikov, In: M. Mashlan, R. Zboril (Eds.), Proceedings of the International Conference "Mössbauer Spectroscopy in Materials Science 2008", AIP Conference Proceedings, Melville, New York, 2008, 1070, pp. 122–130.

[39] M.I. Oshtrakh, V.A. Semionkin, V.I. Grokhovsky, O.B. Milder and E.G. Novikov, J. Radioanal. Nucl. Chem. 279 (2009) 833–846.

[40] M.I. Oshtrakh, V.A. Semionkin, O.B. Milder, E.G. Novikov, J. Mol. Struct. 924–926 (2009) 20–26.

[41] M.I. Oshtrakh, V.A. Semionkin, O.B. Milder, E.G. Novikov, Bull. Rus. Acad. Sci.: Phys. 74 (2010) 407–411.

[42] M.I. Oshtrakh, V.A. Semionkin, O.B. Milder, I.V. Alenkina, E.G. Novikov, Spectroscopy 24 (2010) 593–599.

[43] M.I. Oshtrakh, V.A. Semionkin, I.V. Alenkina, O.B. Milder, Spectrochim. Acta, Part A: Molec. and Biomolec. Spectroscopy 79 (2011) 777–783.

[44] M.I. Oshtrakh, V.A. Semionkin, P.G. Prokopenko, O.B. Milder, A.B. Livshits, A.A. Kozlov, Int. J. Biol. Macromol. 29 (2001) 303–314.

[45] M.I. Oshtrakh, V.A Semionkin, O.B. Milder, E.G. Novikov, J. Radioanal. Nucl. Chem. 281 (2009) 63–67.

[46] V.A. Semionkin, M.I. Oshtrakh, O.B. Milder, E.G. Novikov, Bull. Rus. Acad. Sci.: Phys. 74 (2010) 416–420.

[47] M.I. Oshtrakh, V.A. Semionkin, Spectrochim. Acta, Part A: Molec. and Biomolec. Spectroscopy 100 (2013) 78–87.

[48] M. Koralewski, M. Pochylski, J. Gierszewski, J. Nanopart. Res. 15 (2013) 1902.

[49] M.I. Oshtrakh, I.V. Alenkina, S.M. Dubiel, V.A. Semionkin, J. Mol. Struct. 993 (2011) 287–291.

[50] I.V. Alenkina, M.I. Oshtrakh, Yu.V. Klepova, S.M. Dubiel, N.V. Sadovnikov, V.A. Semionkin, Spectrochim. Acta, Part A: Molec. and Biomolec. Spectroscopy 100 (2013) 88–93.

[51] T.G. St. Pierre, S.H. Bell, D.P.E. Dickson, S. Mann, J. Webb, G.R. Moore, R.J.P. Williams, Biochim. Biophys. Acta 870 (1986) 127–134.

[52] D.E. Madsen, M.F. Hansen, J. Bendix, S. Mørup, Nanotechnol. 19 (2008) 315712.

[53] F.M. Michel, V. Barrón, J. Torrent, M.P. Morales, C.J. Serna, J.-F. Boily, Q. Liu, A. Ambrosini, A.C. Cismasu, G.E. Brown, Proc. Nat. Acad. Sci. 107 (2010) 2787–2792.

[54] R.S. de Biasi, T.C. Devezas, J. Appl. Phys. 49 (1978) 2466–2469.

[55] B.P. Weiss, S.S. Kim, J.L. Kirschvink, R.E. Kopp, M. Sankaran, A. Kobayashi, A. Komeili, Earth Planet. Sci. Lett. 224 (2004) 73–89.

[56] R.E. Siqueira, M.M. Andrade, D.F. Valezi, C.E.A. Carneiro, J.P.P. Pinese, A.C.S. da Costa, D.A.M. Zaia, R. Ralisch, W.M. Pontuschka, C.L.B. Guedes, E. Di Mauro, Appl. Clay Sci. 53 (2011) 42–47.

[57] P.L. Hall, B.R. Angel, J.P.E. Jones, J. Magn. Res. 15 (1974) 64–68.

Table 1. Chemical composition of Ferum Lek and Maltofer® samples.

Sample	**Element**	**Weight %**	**σ (wt.%)**
Ferrum Lek	C	27.86	0.38
	O	40.94	0.37
	Na	1.57	0.06
	Mg	0.61	0.04
	Si	0.80	0.05
	Cl	3.22	0.09
	Fe	24.99	0.53
	Total	100	
Maltofer®	C	22.13	0.50
	O	36.16	0.45
	Na	2.55	0.09
	Cl	5.24	0.15
	Fe	33.92	0.66
	Total	100	

Table 2. Mössbauer parameters obtained from the best fits of the Mössbauer spectra of the human liver ferritin, Maltofer® and Ferrum Lek measured with the high velocity resolution at 295 and 90 K.

Sample	**T, K**	**No[a]**	**δ, mm/s**	**ΔE_Q, mm/s**	**Γ, mm/s**	**S, %**
Ferritin	295	1	0.374±0.001	0.407±0.002	0.276±0.003	26.31
		2	0.372±0.001	0.618±0.001	0.258±0.003	31.16
		3	0.366±0.001	0.859±0.001	0.283±0.003	26.62
		4	0.360±0.001	1.156±0.003	0.343±0.004	15.91
Maltofer®	295	1	0.368±0.001	0.409±0.002	0.233±0.003	15.07
		2	0.370±0.001	0.605±0.001	0.254±0.003	33.41
		3	0.366±0.001	0.856±0.001	0.304±0.003	35.70
		4	0.359±0.001	1.130±0.002	0.261±0.004	10.52
		5	0.344±0.002	1.430±0.006	0.320±0.008	5.30
Ferrum Lek	295	1	0.366±0.001	0.429±0.001	0.245±0.003	20.28
		2	0.368±0.001	0.628±0.001	0.249±0.003	33.84
		3	0.363±0.001	0.877±0.001	0.278±0.003	30.34
		4	0.358±0.001	1.137±0.002	0.233±0.004	9.15
		5	0.344±0.001	1.424±0.005	0.312±0.006	6.39
Ferritin	90	1	0.490±0.002	0.416±0.012	0.340±0.012	26.66
		2	0.480±0.001	0.657±0.018	0.345±0.037	34.89
		3	0.475±0.002	0.918±0.027	0.353±0.042	23.18
		4	0.460±0.003	1.215±0.027	0.433±0.017	15.26
Maltofer®	90	1	0.479±0.001	0.452±0.001	0.303±0.003	15.77
		2	0.472±0.001	0.647±0.002	0.372±0.003	32.87
		3	0.465±0.001	0.867±0.002	0.415±0.003[b]	35.33
		4	0.448±0.001	1.171±0.002	0.339±0.003[b]	10.74
		5	0.410±0.002	1.525±0.005	0.421±0.003[b]	5.29
Ferrum Lek	90	1	0.479±0.001	0.475±0.003	0.311±0.003	20.59
		2	0.477±0.001	0.683±0.002	0.358±0.004	33.46
		3	0.465±0.001	0.902±0.002	0.396±0.003[b]	30.16
		4	0.450±0.001	1.150±0.006	0.331±0.003[b]	9.00
		5	0.421±0.002	1.442±0.009	0.406±0.003[b]	6.80

[a]Numbers of components correspond to components' numbers in Mössbauer spectra in Fig. 4.

[b]Fixed parameter.

Table 3. Mössbauer parameters obtained from the best fits of the Mössbauer spectra of the human liver ferritin, Maltofer® and Ferrum Lek measured with the low velocity resolution at 40 and 20 K.

Sample	T, K	No[a]	δ, mm/s	ΔE_Q, mm/s	H_{eff}, kOe	Γ, mm/s	S, %
Maltofer®	40	1	0.43±0.12	–0.12±0.12	411.8±3.6	0.61±0.24	16
		2	0.33±0.12	–0.01±0.12	381.3±6.1	0.77±0.26	16
		3	0.70±0.12	–0.79±0.16	327.4±6.5	0.75±0.39	8
		4	0.36±0.12	–0.33±0.12	286.0±4.3	0.77±0.26	8
		5	0.17±0.12	–0.15±0.12	174.1±3.5	0.78±0.24	15
		6	0.42±0.12	0.66±0.12	–	0.58±0.24	31
		7	0.50±0.12	1.64±0.22	–	0.51±0.24	6
Ferrum Lek	40	1	0.43±0.12	–0.08±0.12	411.3±3.5	0.44±0.24	8
		2	0.40±0.12	–0.12±0.12	387.2±3.5	0.78±0.24	20
		3	0.57±0.12	–0.34±0.12	342.8±3.5	0.78±0.24	10
		4	0.50±0.12	–0.48±0.12	288.9±3.5	0.78±0.24	12
		5	0.17±0.12	–0.43±0.12	172.9±3.5	0.78±0.24	13
		6	0.44±0.12	0.65±0.12	–	0.60±0.24	28
		7	0.37±0.12	1.28±0.12	–	0.64±0.24	9
Ferritin	20	1	0.38±0.12	–0.69±0.22	344.6±8.0	0.96±0.39	10
		2	0.42±0.12	0.48±0.12	–	0.51±0.24	72
		3	0.43±0.12	0.94±0.12	–	0.41±0.24	18
Maltofer®	20	1	0.45±0.12	–0.12±0.12	417.9±3.5	0.60±0.24	28
		2	0.46±0.12	–0.15±0.12	393.1±3.5	0.66±0.24	20
		3	0.43±0.12	–0.03±0.12	366.1±3.5	0.60±0.24	11
		4	0.50±0.12	–0.06±0.12	332.6±3.5	0.54±0.24	7
		5	0.55±0.12	0.03±0.12	296.8±3.8	0.77±0.24	8
		6	0.69±0.12	–0.12±0.12	220.2±4.8	0.78±0.26	6
		7	0.73±0.12	–0.28±0.12	157.7±5.2	0.78±0.24	6
		8	0.43±0.12	0.75±0.12	–	0.78±0.24	14
Ferrum Lek	20	1	0.44±0.12	–0.13±0.12	416.8±3.5	0.61±0.24	30
		2	0.45±0.12	–0.20±0.12	393.3±3.5	0.56±0.24	17
		3	0.45±0.12	–0.16±0.12	369.0±3.5	0.57±0.24	10
		4	0.47±0.12	–0.09±0.12	340.3±3.5	0.69±0.24	10
		5	0.46±0.12	–0.03±0.12	303.7±3.5	0.70±0.24	8
		6	0.45±0.12	–0.29±0.12	215.7±5.4	0.78±0.24	6
		7	0.66±0.12	–0.25±0.12	155.7±4.4	0.80±0.24	6
		8	0.42±0.12	0.79±0.12	–	0.78±0.24	13

[a]Numbers of components correspond to components' numbers in Mössbauer spectra in Figs. 7 and 8.

FIGURE LEGENDS

Fig. 1. Scanning electron microscopy image of Maltofer® (***a***) and X-ray diffraction patterns of human liver ferritin (***b***), Ferrum Lek (***c***) and Maltofer® (***d***). Arrows indicate peaks positions for ferrihydrite (***F***) and akaganéite (***A***).

Fig. 2. Transmission electron microscopy image of human liver ferritin sample (***a***) with distribution of ferritin iron core sizes determined using 50 particles (***b***) and transmission electron microscopy images of Ferrum Lek (***c***) and Maltofer® (***d***) samples.

Fig. 3. Thermogravimetry of human liver ferritin (***a***), Ferrum Lek (***b***) and Maltofer® (***c***).

Fig. 4. Magnetization curves for human liver ferritin (***a***), Ferrum Lek (***b***, ***d***) and Maltofer® (***c***, ***e***, ***f***). PM is a paramagnetic (or superantiferromagnetic) linear component, M_s is a saturation magnetization.

Fig. 5. Mössbauer spectra of human liver ferritin (***a, b***), Ferrum Lek (***c, d***) and Maltofer® (***e, f***) measured at 295 K (***a, c, e***) and 90 K (***b, d, f***) with the high velocity resolution (in 4096 channels). Indicated components are the results of the best consistent fits. Examples of non-linear differential spectra for the fits using one, two and three quadrupole doublets are inserted into the spectrum of human liver ferritin (***a***). Differential spectra are shown below.

Fig. 6. Histograms of the relative areas of the components in the Mössbauer spectra of human liver ferritin (***a***), Ferrum Lek (***b***) and Maltofer® (***c***) measured at 295 K (■) and 90 K (□). Numbers of spectral components are corresponding to those in Fig. 4.

Fig. 7. Mössbauer spectra of Maltofer® (***a***) and Ferrum Lek (***b***) measured at 90 K with the high velocity resolution in a large velocity range (***a*** – in 4096 channels, ***b*** – presented in 2048 channels) and iron-polymaltose complex measured with the low velocity resolution at 78 K in a large velocity range adopted from [29] (***c***). Indicated components are the results of the best fits. Differential spectra are shown below.

Fig. 8. Mössbauer spectra of human liver ferritin (***a***), Maltofer® (***b***) and Ferrum Lek (***c***) measured

at 20 K with the low velocity resolution (in 250 channels) on the direct motion. Indicated components are the results of the best fits. Differential spectra are shown below.

Fig. 9. Mössbauer spectra of Maltofer® (***a***), Ferrum Lek (***b***) measured with the low velocity resolution (in 250 channels) on the direct motion at 40 K and iron-polymaltose complex measured with the low velocity resolution at 45 K adopted from [29] (***c***). Indicated components are the results of the best fits. Differential spectra are shown below.

Fig. 10. X-band EPR spectra (derivative of microwave absorption as a function of the flux density of the sweeping magnetic field) of human liver ferritin, Maltofer® and Ferrum Lek recorded at $T \approx 293(2)$ K, and the corresponding fit envelopes with subcomponents. The magnetic field axis has been scaled to correspond to a measuring frequency of $f = 9.8$ GHz. The actual measuring frequencies were 9.8604 GHz (ferritin), 9.3235 GHz (Maltofer®) and 9.8658 GHz (Ferrum Lek). The magnetic field value belonging to the spectroscopic splitting factor of $g = 2$ is marked by a vertical dashed line.

Fig. 11. X-band EPR spectra of human liver ferritin measured at the given temperatures and displayed for the magnetic field range of 500–2500 G, showing that the intensity of the paramagnetic signal at $g \approx 4.2$, referring to solitary iron ions bonded to the ferritin shell, tends to increase with decreasing temperature such that it becomes discernible below room temperature. The magnetic field axis has been scaled to correspond to a measuring frequency of $f = 9.8$ GHz. The actual measuring frequency was 9.3347 GHz.

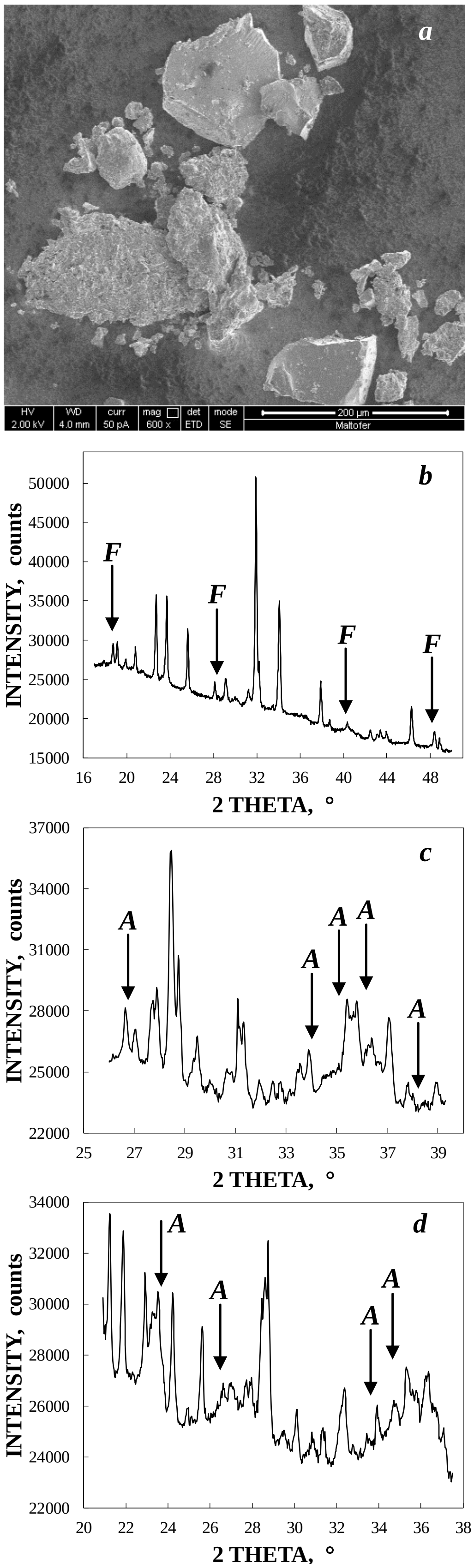
a
HV 2.00 kV
WD 4.0 mm
curr 50 pA
mag 600 x
det ETD
mode SE
200 µm
Maltofer
b
INTENSITY, counts
50000
45000
40000
35000
30000
25000
20000
15000
16 20 24 28 32 36 40 44 48
2 THETA, °
F
F
F
F
c
INTENSITY, counts
37000
34000
31000
28000
25000
22000
25 27 29 31 33 35 37 39
2 THETA, °
A
A
A
A
A
d
INTENSITY, counts
34000
32000
30000
28000
26000
24000
22000
20 22 24 26 28 30 32 34 36 38
2 THETA, °
A
A
A
A

Fig. 1.

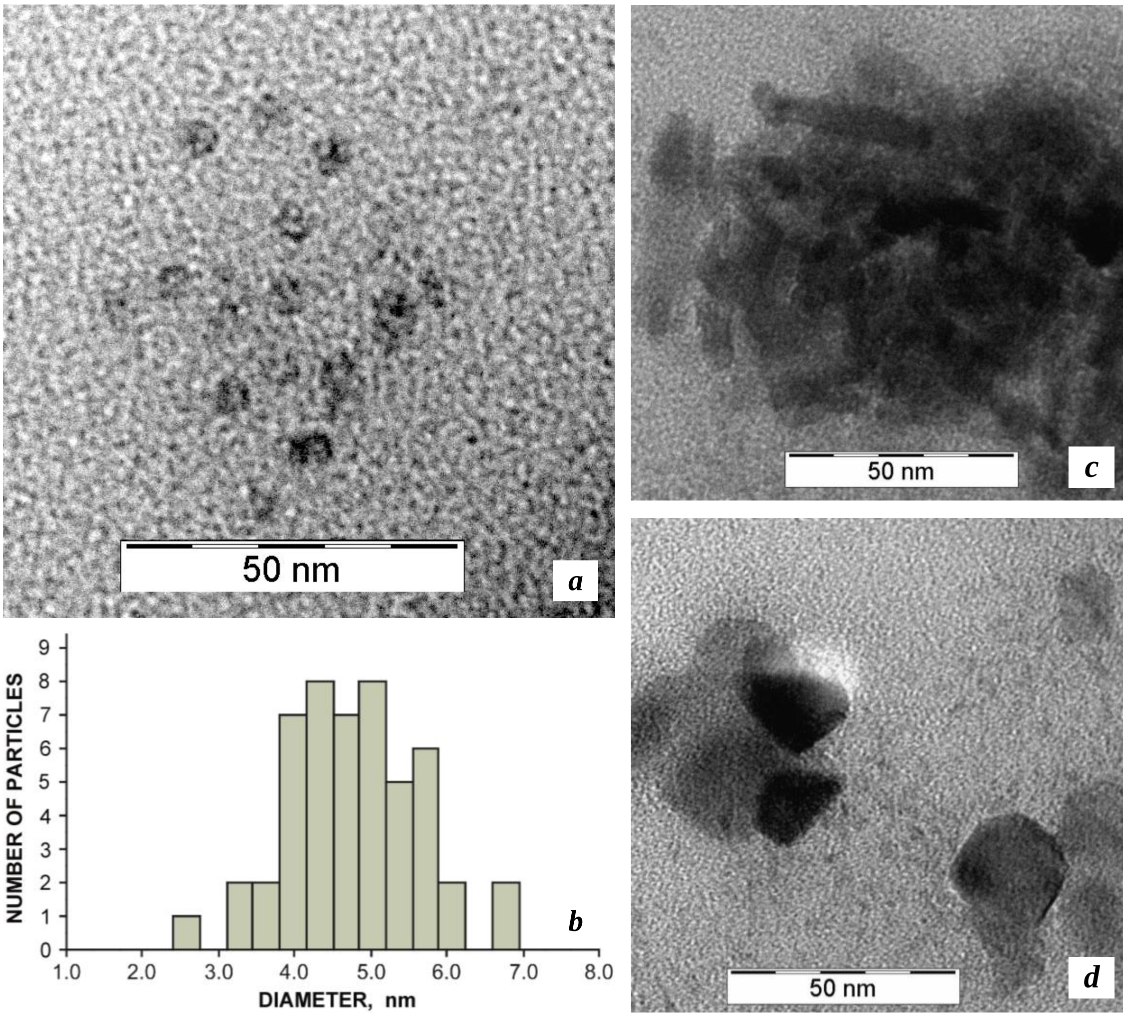

Fig. 2.

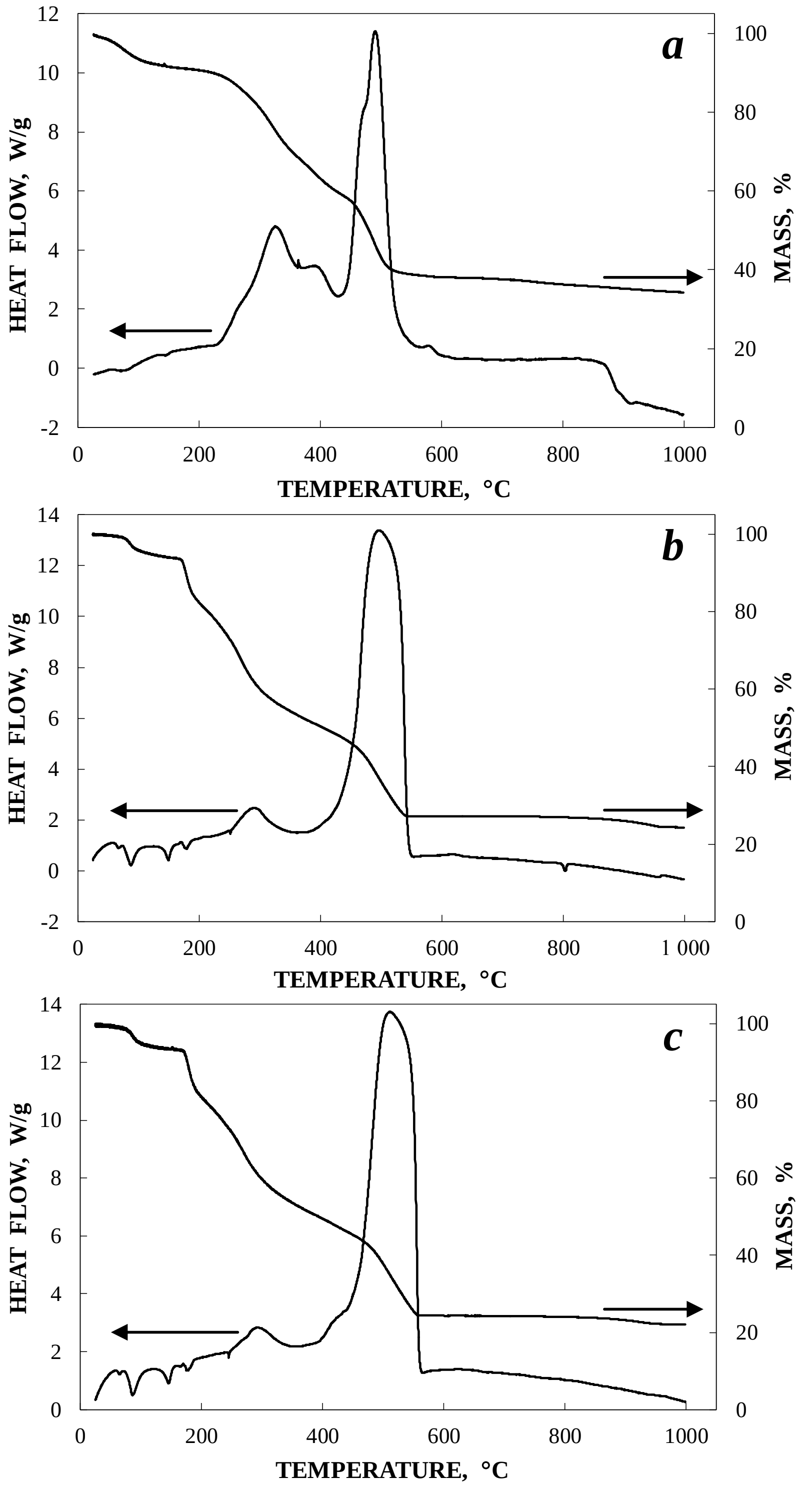
a
HEAT FLOW, W/g
MASS, %
TEMPERATURE, °C
12
10
8
6
4
2
0
-2
100
80
60
40
20
0
0
200
400
600
800
1000
b
HEAT FLOW, W/g
MASS, %
TEMPERATURE, °C
14
12
10
8
6
4
2
0
-2
100
80
60
40
20
0
0
200
400
600
800
1 000
c
HEAT FLOW, W/g
MASS, %
TEMPERATURE, °C
14
12
10
8
6
4
2
0
100
80
60
40
20
0
0
200
400
600
800
1000

Fig. 3.

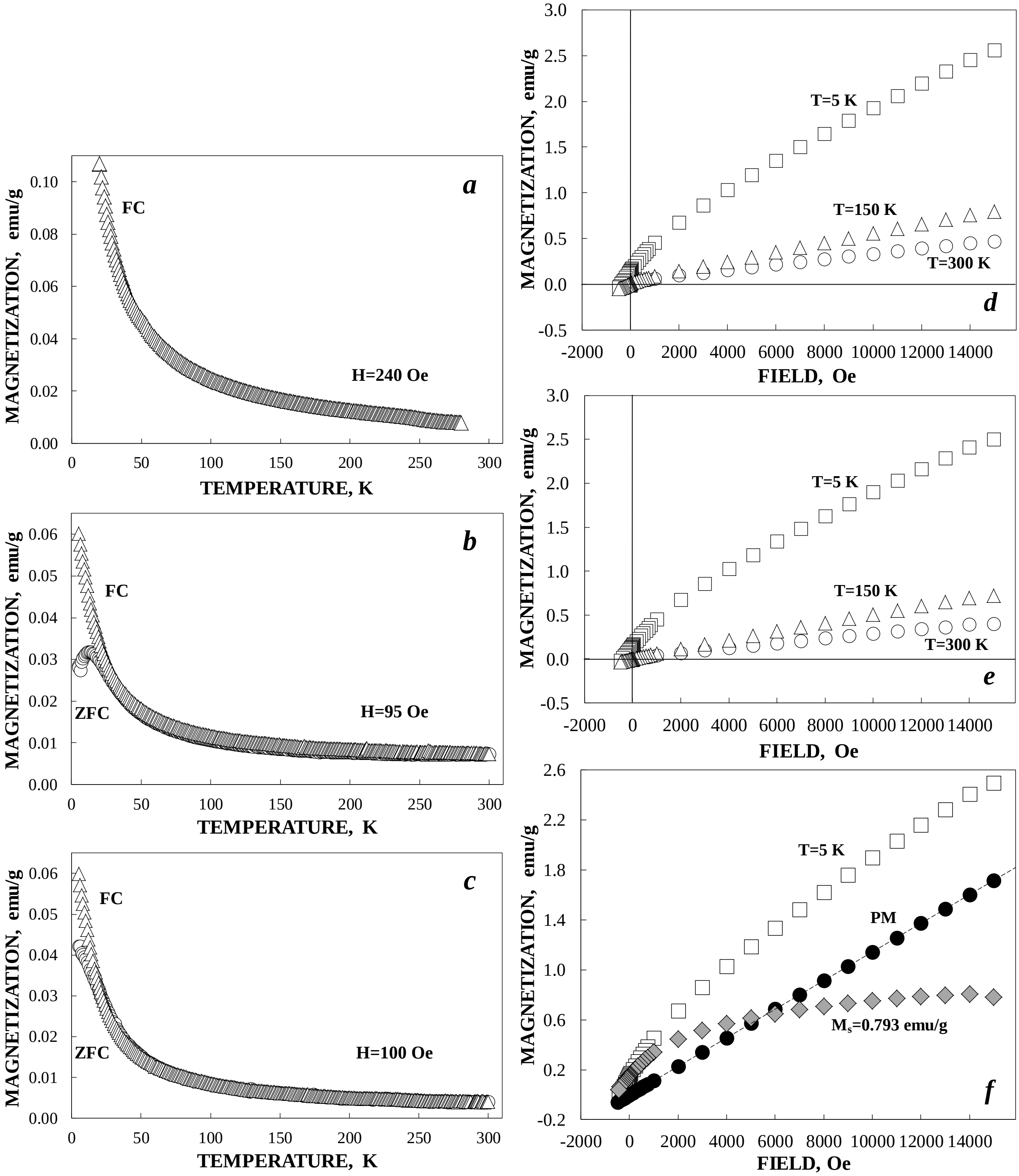
a
FC
H=240 Oe
MAGNETIZATION, emu/g
TEMPERATURE, K
b
FC
ZFC
H=95 Oe
MAGNETIZATION, emu/g
TEMPERATURE, K
c
FC
ZFC
H=100 Oe
MAGNETIZATION, emu/g
TEMPERATURE, K
d
T=5 K
T=150 K
T=300 K
MAGNETIZATION, emu/g
FIELD, Oe
e
T=5 K
T=150 K
T=300 K
MAGNETIZATION, emu/g
FIELD, Oe
f
T=5 K
PM
Ms=0.793 emu/g
MAGNETIZATION, emu/g
FIELD, Oe

Fig. 4.

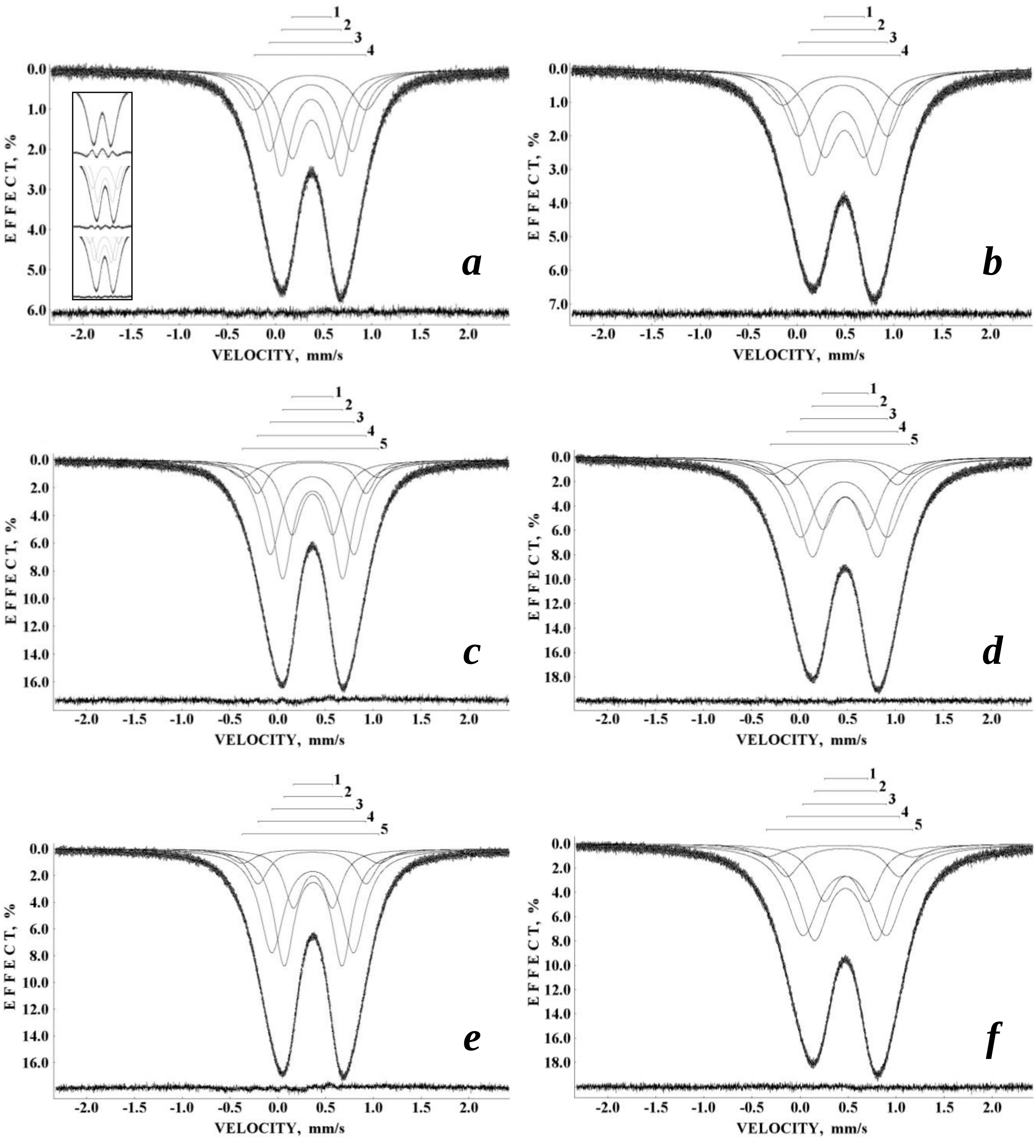

Fig. 5.

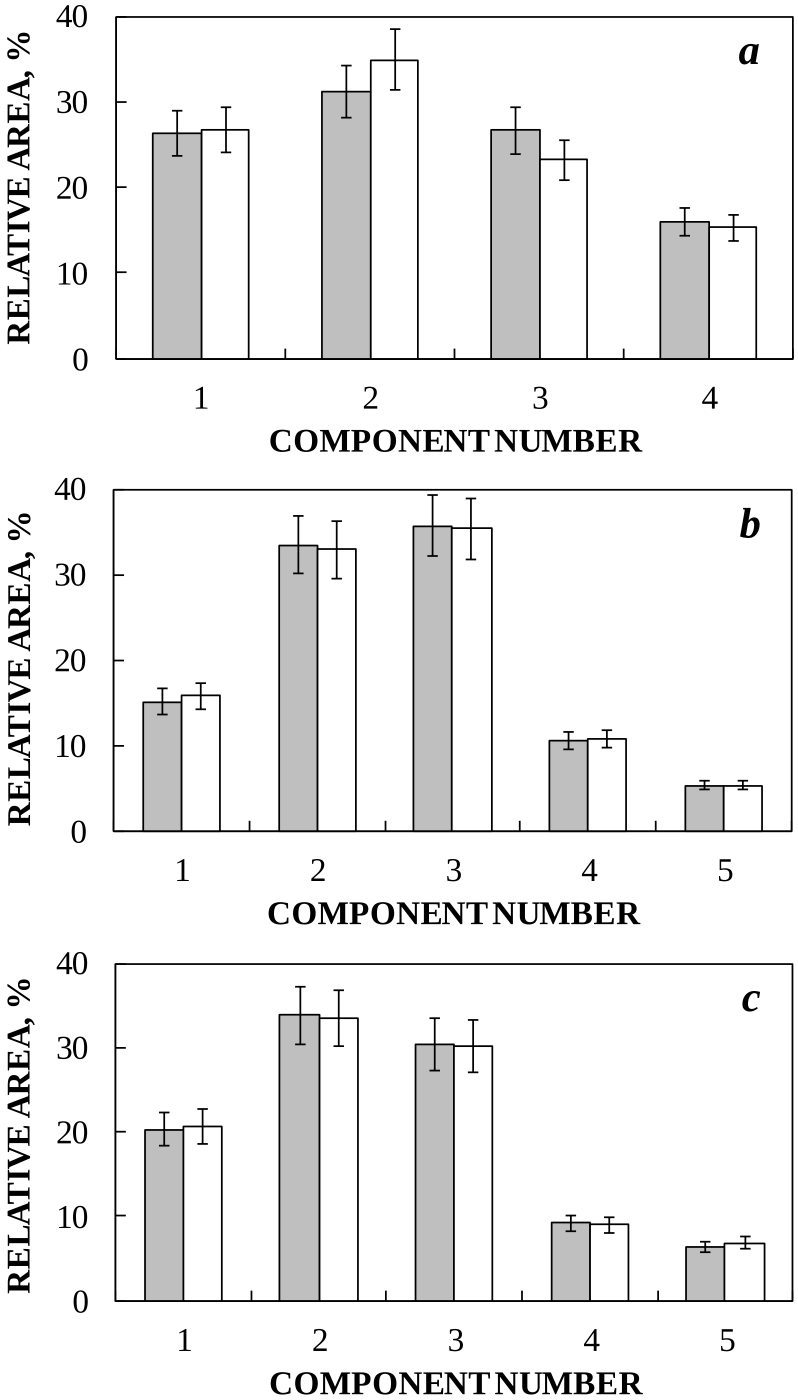

Fig. 6.

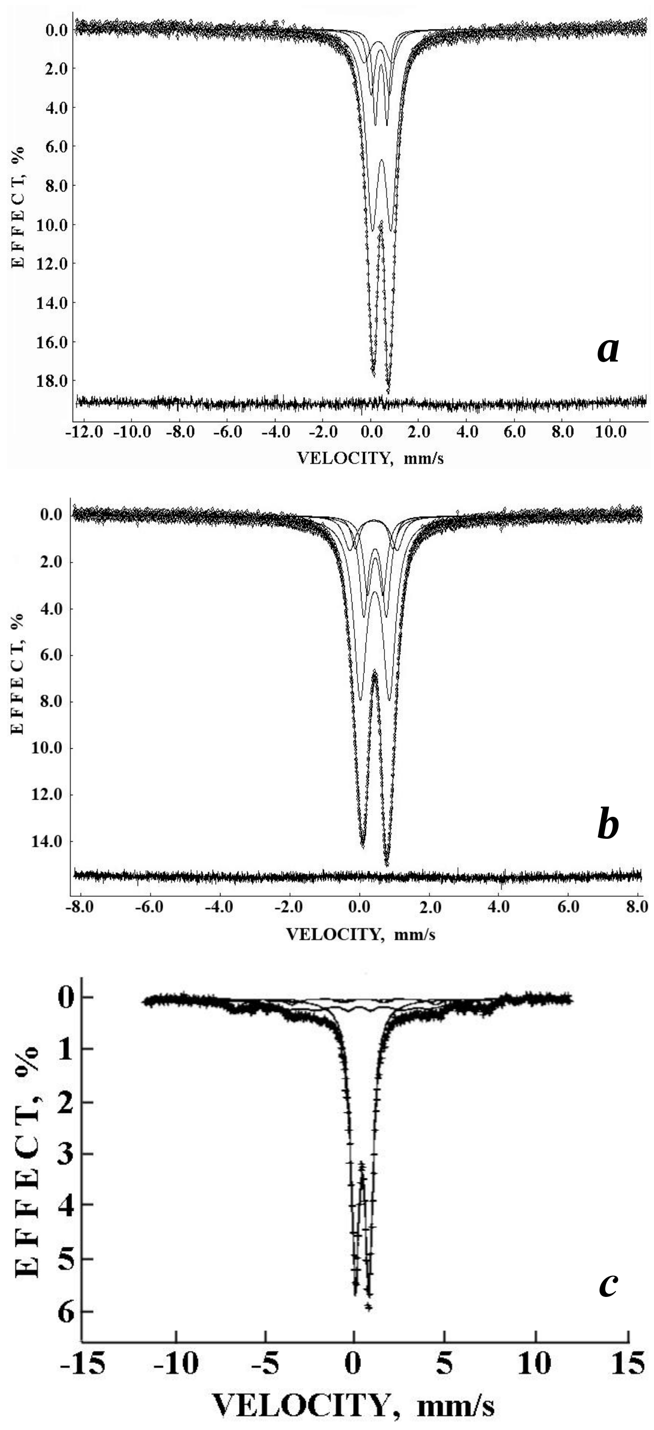
EFFECT, %
VELOCITY, mm/s
a
EFFECT, %
VELOCITY, mm/s
b
EFFECT, %
VELOCITY, mm/s
c

Fig. 7.

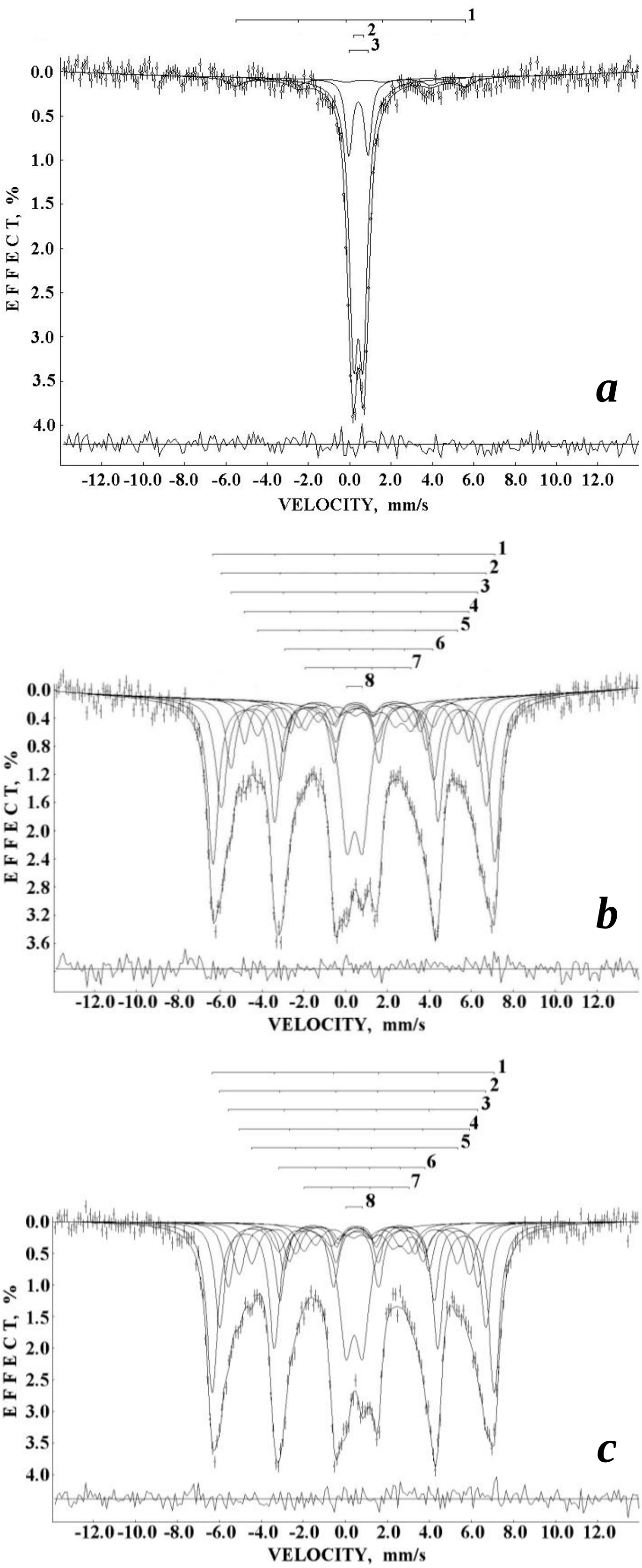
a
b
c
EFFECT, %
VELOCITY, mm/s
-12.0 -10.0 -8.0 -6.0 -4.0 -2.0 0.0 2.0 4.0 6.0 8.0 10.0 12.0

Fig. 8.

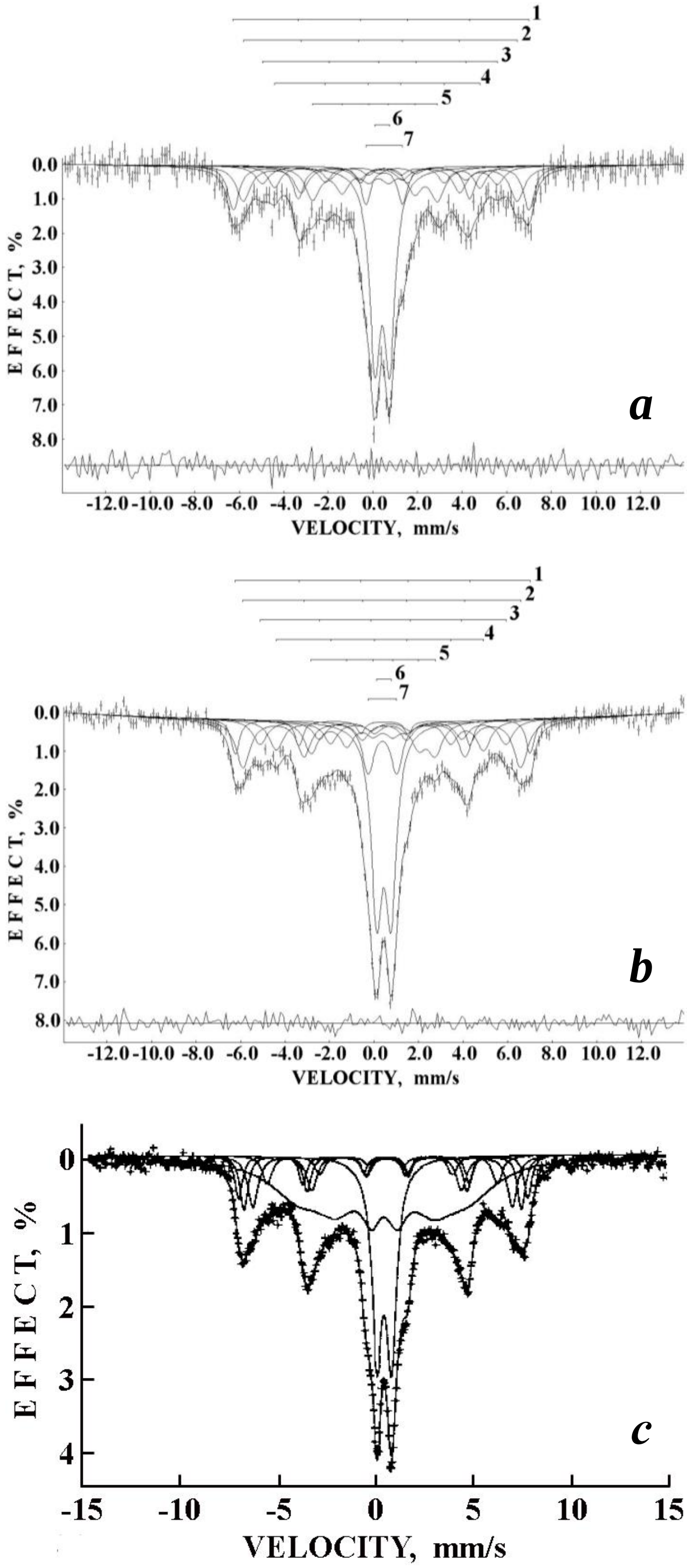
1
2
3
4
5
6
7
0.0
1.0
2.0
3.0
4.0
5.0
6.0
7.0
8.0
EFFECT, %
a
-12.0 -10.0 -8.0 -6.0 -4.0 -2.0 0.0 2.0 4.0 6.0 8.0 10.0 12.0
VELOCITY, mm/s
1
2
3
4
5
6
7
0.0
1.0
2.0
3.0
4.0
5.0
6.0
7.0
8.0
EFFECT, %
b
-12.0 -10.0 -8.0 -6.0 -4.0 -2.0 0.0 2.0 4.0 6.0 8.0 10.0 12.0
VELOCITY, mm/s
0
1
2
3
4
EFFECT, %
c
-15 -10 -5 0 5 10 15
VELOCITY, mm/s

Fig. 9.

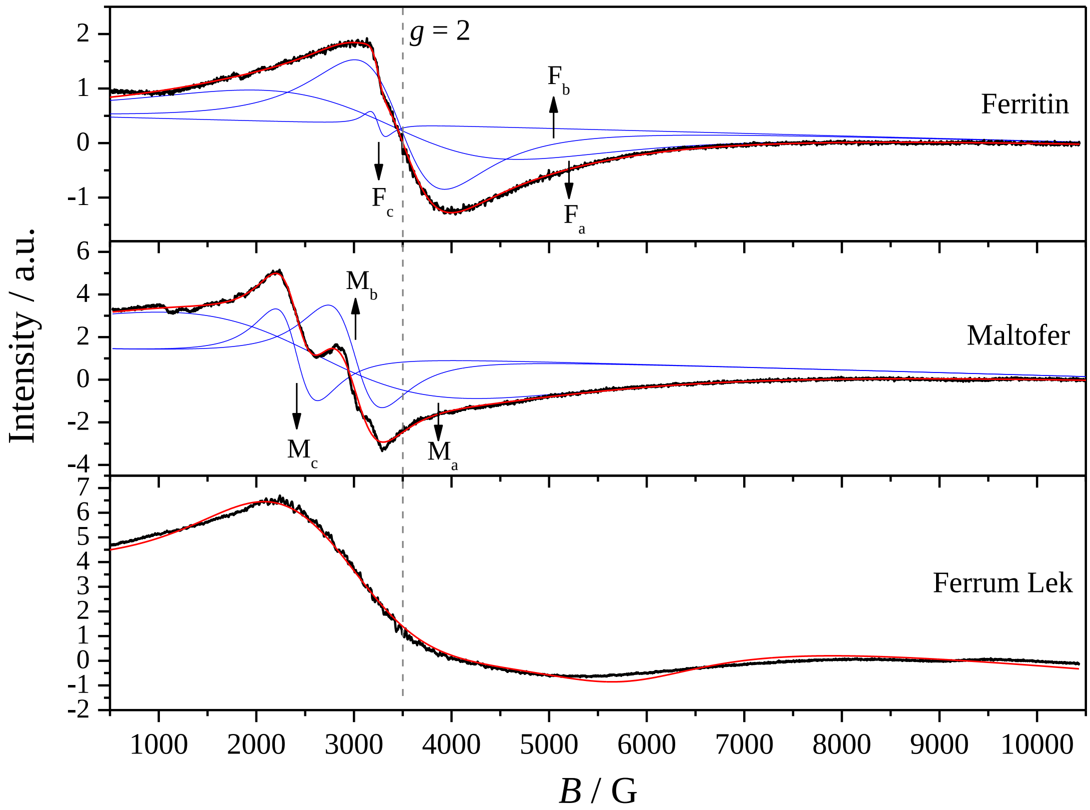
g = 2
Ferritin
F_b
F_c
F_a
Maltofer
M_b
M_c
M_a
Ferrum Lek
Intensity / a.u.
B / G

Fig. 10.

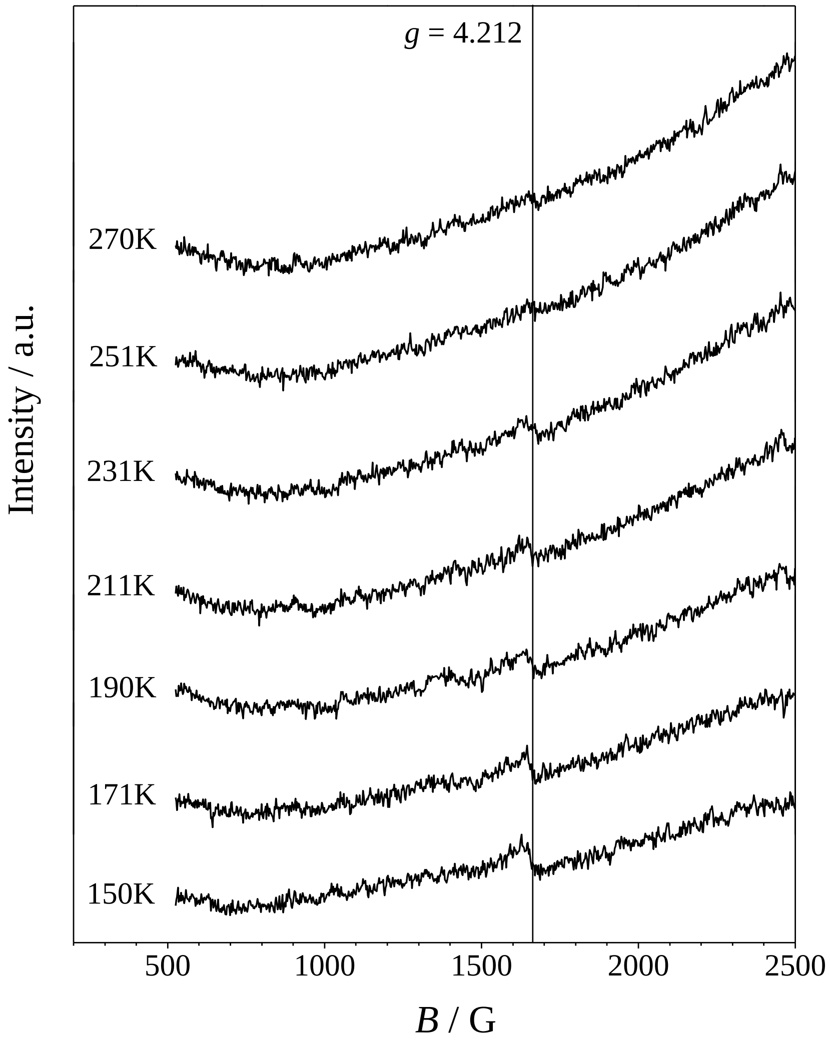
g = 4.212
270K
251K
231K
211K
190K
171K
150K
Intensity / a.u.
500
1000
1500
2000
2500
B / G

Fig. 11.